Quantifying the Complementarity of Wind Turbines and Distributed Photovoltaics for Coordinated Primary Frequency Control

Songyan Zhang[1], Di Liu[1], Chao Lu[1]
[1]*Department of Electrical Engineering*, *Tsinghua University*, Beijing, China
luchao@tsinghua.edu.cn

Abstract——**Exploiting the frequency support capability (FSC) of small-scale renewable energy sources (RES) can significantly enhance system frequency stability. However, the FSC of wind turbines (WTs) is limited by complex safety constraints and naturally asymmetric for up-regulation (UR) and down-regulation (DR) scenarios. Besides, the secondary frequency change (SFC) issue due to rotor speed recovery has long restricted WT's participation in primary frequency control (PFC). To provide symmetric droop support and mitigate SFC, this paper explores the complementarity of WTs and distributed photovoltaics (DPVs), and then propose an aggregated WT-DPV FSC assessment model integrating WT dynamics and system frequency response (SFR) dynamics. To solve this model, the nonlinear WT dynamics and safety constraints are converted into piecewise-linear (PWL) constrained state transition constraints; while the interaction between SFR dynamic and WT-DPV droop gains is handled by an iterative solution method. Moreover, the SFC is mitigated by strategic DPV-aided WT exit. A comprehensive case study is presented to verify the assessment model's accuracy and solution efficiency, and the benefits of WT-DPV coordination.**

Keywords—wind turbine, distributed photovoltaics, droop gain, primary frequency control, system frequency response model.

I. INTRODUCTION

The large-scale integration of renewable energy sources (RES) has led to a continuous decline in the effective inertia and exacerbated real-time power imbalance, posing a severe threat to frequency stability [1]. To mitigate the negative impacts of RES integration, it is essential to leverage RES units to provide primary frequency control (PFC) [2]. This paper focuses on coordinated PFC from wind turbines (WTs) and distributed photovoltaic (DPVs) and the quantification of the hybrid RES station's frequency support capacity (FSC), which is defined as the maximum available droop gain w.r.t. a predefined load step change disturbance event.

PFC strategies for WTs can be broadly classified into two categories: stepwise control and frequency-based control. Stepwise control pre-defines the WTs' power trajectory during frequency event to fully utilize their rotor kinetic energy (RKE)-based FSC [3]. However, limited by the open-loop nature, its performance can deteriorate if the actual frequency trajectory deviates from expectations. Conversely, Frequency-based control adds an auxiliary PFC loop in addition to the rotor speed control loop to provide power support [4], [5], [6]. This auxiliary loop uses frequency measurement as feedback, where the droop and inertia gains should be carefully designed.

Quantifying the feasible region for the PFC gains of WTs faces two main challenges. First, the inherent nonlinearity of WT dynamics complicates the inclusion of WT state transition in FSC assessment model, which is necessary for ensuring WT safety during PFC. Second, a WT's maximum PFC gain and the system frequency response (SFR) dynamics are mutually influencing. This interaction introduces nonlinear terms into the FSC assessment model. In [7], a conservative droop gain boundary is derived by neglecting WT-SFR interaction. Ref.[8] establishes a mapping from droop-inertia gain to the initial and final operating states of WT to roughly guarantee safety. In [9], the state transition process of WT during PFC is converted into a set of high-dimensional linear time-coupled constraints. While the assessment models in [8] and [9] solved the two challenges to some extent, the dimension-lifting nature of Koopman Operator has limited the model applicability in scenario where heterogeneous WTs exist. The change in SFR parameters cannot be flexibly included as well.

Furthermore, there are two more issues to be considered for WT-FSC utilization. First, WT-FSC is based on RKE and thereby temporary. After a period, WTs must exit PFC to ensure rotor speed safety, risking secondary frequency change (SFC). Second, WTs typically offer larger up-regulation (UR) than down-regulation (DR) due to high base rotor speeds. However, from the perspective of frequency-constrained dispatch, a RES station's PFC supply is preferred to be symmetric [10]. It is noted that DPVs with power reserve control can flexibly shape its UR/DR capacity by adjusting the baseline power [11]. Thus, the aggregation of WT and DPV's asymmetric FSC can create symmetric and larger droop support to the bulk grid. As for the SFC issue, DPVs can continuously increase/decrease its output as WTs exit PFC, thereby smoothing the disturbance to system frequency.

In summary, considering the strong potential of WTs and DPVs in synergistically providing PFC, this paper proposes a quantitative assessment model for aggregated WT-DPV FSC. The main contributions are: i) Utilize piecewise linearization (PWL) and iterative solution method to ensure the solvability and computational efficiency of the assessment model; ii) Reveal and verify the benefits of WT-DPV coordination in terms of increased droop supply and SFC mitigation.

II. BASIC MODELING OF WT IN PFC SCENARIO

A. *WT Dynamic and Safety Constraint Modeling*

For a doubly-fed induction generator (DFIG)-type WT, its rotor dynamic of can be described by the one-mass model in (1), where $2H_w$ is the inertia, ω_r is the rotor speed, P_{m} is the mechanical power, P_{e} is the electric power. While P_{e} is determined by the WT's control logic, P_{m} is jointly affected by rotor speed, pitch angle β and the wind speed v_w. According to aerodynamic research [4], [9], P_{m} is calculated by (2), where ρ is air density, R_w is blade radius, λ is tip speed ratio, λ_i is intermediate variable and $C_p(\lambda, \beta)$ is the power coefficient.

This work was supported by the Youth Program of the National Natural Science Foundation of China under Grant No.52407116.

XXX-X-XXXX-XXXX-X/XX/$XX.00 ©20XX IEEE
979-8-3315-8138-1

$$2H_{\mathrm{WT}} \cdot \dot{\omega}_r = (P_m - P_e) / \omega_r \tag{1}$$

$$P_m(\omega_r, \beta, v_w) = 0.5\rho\pi R_w^2 v_w^3 C_p(\lambda, \beta)$$

$$\begin{cases} \lambda = \dfrac{\omega_r R_w}{v_w}, \dfrac{1}{\lambda_i} = \dfrac{1}{\lambda + 0.08\beta} - \dfrac{0.035}{1+\beta^3} \\ C_p(\lambda, \beta) = 0.22 \cdot (\dfrac{116}{\lambda_i} - 0.4\beta - 5) e^{-\frac{12.5}{\lambda_i}} \end{cases} \tag{2}$$

The safe operation of a WT should satisfy multiple constraints [6], [9]. In (3), we list the rotor speed limit, electromagnetic torque limit and power limit in order, where the typical limit values $\omega_{r,\min}$= 0.7 p.u., $\omega_{r,\max}$= 1.2 p.u., $T_{e,\max}$= 1.2 p.u. and $P_{e,\max}$= 1.2 p.u.. Furthermore, the rotor-side converter (RSC) capacity limit is presented in (4), where P_r is RSC power. A notable economic benefit of DFIG is that it necessitates a reduced RSC capacity S_r= 0.3 p.u.. Assuming that the WT does not generate reactive power, then we have $P_{r,\max} = \sqrt{S_r^2 - Q_r^2} = 0.3$ p.u. .

$$\omega_{r,\min} \le \omega_r \le \omega_{r,\max}, T_e = P_e / \omega_r \le T_{e,\max}, 0 \le P_e \le P_{e,\max} \tag{3}$$

$$-P_{r,\max} \le P_r \le P_{r,\max}, P_r = P_e \cdot (1 - 1/\omega_r) \tag{4}$$

B. Electric Power Composition of WTs in PFC

The electric power P_e of a WT consists of two parts, namely the rotor speed tracking (RST) power $P_{e,\mathrm{rst}}$ generated by RST loop and the support power $\Delta P_{e,\sup}$ generated by PFC loop. The objective of $P_{e,\mathrm{rst}}$ is to capture wind energy and maintain rotor speed, while $\Delta P_{e,\sup}$ is used to support system frequency. We define UR as the case where $\Delta f < 0$ and the WT's RKE is released, and DR as the opposite. Their relationship is summarized in (5), where k_{rst} is RST gain, $k_{\mathrm{up/dn}}^{\mathrm{WT}}$ are UR/DR droop gains.

$$P_e = P_{e,\mathrm{rst}} + \Delta P_{e,\sup} = \begin{cases} k_{\mathrm{rst}}\omega_r^2 - k_{\mathrm{up}}^{\mathrm{WT}}\Delta f, & \Delta f < 0 \\ k_{\mathrm{rst}}\omega_r^2 - k_{\mathrm{dn}}^{\mathrm{WT}}\Delta f, & \Delta f > 0 \end{cases} \tag{5}$$

The principle behind using the convex function $k_{\mathrm{rst}}\omega_r^2$ for $P_{e,\mathrm{rst}}$ is that, the mechanical power function (2) is concave; therefore, the condition (6) for the asymptotic stability of ω_r is satisfied near the reference rotor speed ω_r^{ref}. The RST gain is calculated by (7), where $\hat{v}_w$ is the estimated wind speed. It can be observed that during PFC, $P_{e,\mathrm{rst}}$ is changing with ω_r, which can weaken the support effect of $\Delta P_{e,\sup}$.

$$P_e < P_m \,\&\, \omega_r < \omega_r^{\mathrm{ref}}; \quad P_e > P_m \,\&\, \omega_r > \omega_r^{\mathrm{ref}} \tag{6}$$

$$k_{\mathrm{rst}} = P_m(\omega_r^{\mathrm{ref}}, \beta^{\mathrm{ref}}, \hat{v}_w) / (\omega_r^{\mathrm{ref}})^2 \tag{7}$$

C. Reformulation of WT Dynamic and Safety Constraint

As depicted in Fig. 1, the P_e-ω_r trajectory of a WT should be always constrained within the non-convex safety region enclosed by four limits (the blue shaded area). By converting the left RSC constraint to a tangent line, the original safety region can be substituted by a convex hexagon. Next, we can split the convex hexagon into three sub-regions with rotor speed ranges of $\Omega_{\mathrm{SR},1}$:=$\omega_{r,1}$~$\omega_{r,2}$, $\Omega_{\mathrm{SR},2}$:=$\omega_{r,2}$~$\omega_{r,3}$ and $\Omega_{\mathrm{SR},3}$:=$\omega_{r,3}$~$\omega_{r,4}$, respectively. For each sub-region, its scope can be described by inequality in (8), where the six parameters $\{a_{\mathrm{SR},c}, b_{\mathrm{SR},c} \mid c = 1,2,3\}$ can be obtained by curve-fitting. Finally, a conservative but safe inner approximation of the original safety region is obtained.

$$\omega_r \in \Omega_{\mathrm{SR},c} : 0 \le P_e \le a_{\mathrm{SR},c} \cdot \omega_r^2 + b_{\mathrm{SR},c}, \; c = \{1,2,3\} \tag{8}$$

The reformulation of WT dynamic consists of two steps. First, the rotor dynamic differential equation (1) is converted into the discrete equation (9), where n indicates the n^{th} time step, ω_r^2 is the new state variable. Next, the mechanical power function (2) is reformulated as a PWL function of ω_r^2 in (10). The six parameters $\{a_{\mathrm{M},c}, b_{\mathrm{M},c} \mid c = 1,2,3\}$ should be obtained through regression separately for each WT to precisely model diversified aerodynamic characteristics.

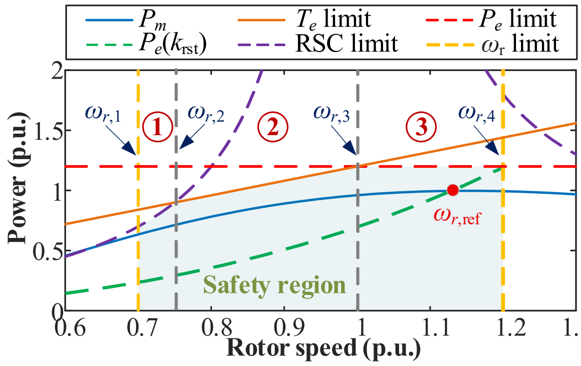

Fig. 1. Illustrative diagram of safety region and rotor speed tracking control.

$$\omega_r^2(n+1) = \omega_r^2(n) + \frac{\Delta t}{H_{\mathrm{WT}}}[P_m(n) - P_e(n)] \tag{9}$$

$$\omega_r(n) \in \Omega_{\mathrm{SR},c} : P_m(n) \approx a_{\mathrm{M},c} \cdot \omega_r^2(n) + b_{\mathrm{M},c}, \; c = \{1,2,3\} \tag{10}$$

III. AGGREGATED WT-DPV FSC ASSESSMENT MODEL

A. SFR Modeling Considering WT-DPV Support

For a short period, the maximum power that a DPV can stably output is denoted as $P_{\max}^{\mathrm{PV}}$. We can define the real-time PV output power in (11), where $P_{\mathrm{base}}^{\mathrm{PV}}$ is base power and $k_{\mathrm{up/dn}}^{\mathrm{PV}}$ are UR/DR droop gains. Then, the constraints for $P_{\mathrm{base}}^{\mathrm{PV}}$ and $k_{\mathrm{up/dn}}^{\mathrm{PV}}$ are defined in (12), where $\Delta f_{\max}$ is the maximum frequency deviation under certain PFC from the RES station.

$$P_e^{\mathrm{PV}} = \begin{cases} P_{\mathrm{base}}^{\mathrm{PV}} - k_{\mathrm{up}}^{\mathrm{PV}}\Delta f, & \Delta f < 0 \\ P_{\mathrm{base}}^{\mathrm{PV}} - k_{\mathrm{dn}}^{\mathrm{PV}}\Delta f, & \Delta f > 0 \end{cases} \tag{11}$$

$$\begin{cases} P_{\mathrm{base}}^{\mathrm{PV}} \in [0, P_{\max}^{\mathrm{PV}}] \\ k_{\mathrm{up}}^{\mathrm{PV}} \le (P_{\max}^{\mathrm{PV}} - P_{\mathrm{base}}^{\mathrm{PV}}) / |\Delta f_{\max}|, \quad k_{\mathrm{dn}}^{\mathrm{PV}} \le P_{\mathrm{base}}^{\mathrm{PV}} / |\Delta f_{\max}| \end{cases} \tag{12}$$

Fig.2 shows the linear SFR dynamic model in [3], [6]. $2H_{\mathrm{SG}}$ and D_{SG} are the equivalent system inertia and damping, respectively. For the aggregated synchronous generator (SG), its turbine-governor dynamic is the first-order link in red box, where R is the inverse droop, T_R is the reheat time constant and F_H is the fraction constant. For DPV, its support power ΔP_{PV} is only determined by Δf and droop gains. However, the WT support power ΔP_{WT} consists of the droop support part and the variation in RST power. As converter-interfaced units, the inner control delay of WT and DPV can be modeled as two first-order loops. Since the timescale of T_{PV} and T_{WT} are much faster than that of rotor dynamics and SFR dynamics [8], we assume that $G_{\mathrm{PV}}(s)$=$G_{\mathrm{WT}}(s)$=1 in the following analysis. The deadband Δf_{db} is usually set as 0.033 Hz, which is negligible in FSC assessment.

B. DPV-aided WT Sequential Exit Strategy

For low-inertia system, it is considered that the frequency has basically stabilized after the disturbance for 15 s [8]. Since step size Δt is set as 0.1 s, the number of time steps in the FSC assessment model is N_s=150. The set of time steps is denoted by $\mathcal{T}_{\sup}$. As discussed in **Section-I**, all WTs exiting PFC and recovering speed simultaneously can lead to serious SFC. To reduce power surges and ensure WT safety, we adopt a sequential exit strategy of two steps. First, at the N_s^{th} time step, each WT sets its droop gain to 0 and RST gain to

$k_{\text{rst}}^{'} = P_m(\omega_r(N_s), \beta^{\text{ref}}, \hat{v}_w) / \omega_r^2(N_s)$, in order to maintain the current rotor speed. Meanwhile, DPVs should release all its remained UR/DR margin in UR/DR event, respectively, in order to reduce power disturbance due to the PFC exit of WTs. Second, every 0.5 seconds, one WT restores its RST gain to the original value k_{rst} in (7), in order to recover to initial rotor speed ω_r^{ref}. Among these, an interval of 0.5 seconds is a value that balances the rotor speed recovery duration and the effectiveness of SFC elimination. The strategy imposes no specific requirements on the RST gain restoration sequence for individual WTs; however, in general, the RST gains of WTs with larger $\left|(k_{\text{rst}}^{'} - k_{\text{rst}}) \cdot \omega_r^2(N_s)\right|$ values are advised to be restored later.

C. Assessment Model Formulation and Its Solution

To construct the aggregated WT-DPV FSC assessment model, we first need to model the interaction between WT-DPV and SFR. Assuming that a step load change $\Delta P_{\text{dis}}(s) = \Delta P_L / s$ happens at t_0=0, the differential equation of [Δf, ΔX] is presented in (13). The initial values of Δf and ΔX are both 0. Since WTs have different initial operating states, their droop gains should be set differently to guarantee operational safety. Denote the set of WTs as $\mathcal{N}_{\text{WT}}$, the aggregate UR/DR WT droop gains are defined in (14). Then, the forward Euler method is used to discretize (13) to obtain a linear state transition equation of Δf in (15).

$$\begin{bmatrix} \Delta\dot{f} \\ \Delta\dot{X} \end{bmatrix} = \begin{bmatrix} -\dfrac{F_H + D_{\text{SG}}R}{2H_{\text{SG}}R} & \dfrac{1}{2H_{\text{SG}}} \\ -\dfrac{1-F_H}{RT_R} & \dfrac{-1}{T_R} \end{bmatrix} \begin{bmatrix} \Delta f \\ \Delta X \end{bmatrix} + \begin{bmatrix} \dfrac{-1}{2H_{\text{SG}}} \\ 0 \end{bmatrix} \Delta P_{\text{total}} \tag{13}$$

where $\Delta P_{\text{total}} = \Delta P_L - \Delta P_{\text{WT}} - \Delta P_{\text{PV}}$

$$k_{\text{up}}^{\text{WT}} = \sum\nolimits_{i\in\mathcal{N}_{\text{WT}}} k_{\text{up},i}^{\text{WT}}, \quad k_{\text{dn}}^{\text{WT}} = \sum\nolimits_{i\in\mathcal{N}_{\text{WT}}} k_{\text{dn},i}^{\text{WT}} \tag{14}$$

$$\begin{cases} \Delta f(n+1) = F_{\text{SFR}}(\Delta P_L, \Delta P_{\text{WT}}(n), \Delta P_{\text{PV}}(n), \Delta f(n), \Delta X(n)) \\ \Delta P_{\text{WT}}(n) = -k_{\text{up/dn}}^{\text{WT}} \Delta f(n) + \sum\nolimits_{i\in\mathcal{N}_{\text{WT}}} k_{\text{rst},i}\left[\omega_{r,i}^2(n) - \omega_{r,i}^2(0)\right] \\ \Delta P_{\text{PV}}(n) = -k_{\text{up/dn}}^{\text{PV}} \Delta f(n) \end{cases} \tag{15}$$

Next, we need to model the transition of each WT's P_e-ω_r trajectory during PFC. For UR scenario (ΔP_L>0), the electric power of WT i is determined by its current rotor speed $\omega_{r,i}^2(n)$ and $\Delta f(n)$ from (15). Then, $P_{e,i}(n)$ is combined with (8)-(10) to represent the constrained P_e-ω_r trajectory during $\mathcal{T}_{\text{sup}}$ in (16). The DR scenario (ΔP_L<0) is similar and presented in (17). Note that $|\Delta P_L|$ are the same for both scenarios.

$$\text{UR scenario}: \begin{cases} P_{e,i}(n) = k_{\text{rst},i}\omega_{r,i}^2(n) - k_{\text{up},i}^{\text{WT}}\Delta f(n), \\ (8),\ (9),\ (10) \end{cases} \tag{16}$$

$$\text{DR scenario}: \begin{cases} P_{e,i}(n) = k_{\text{rst},i}\omega_{r,i}^2(n) - k_{\text{dn},i}^{\text{WT}}\Delta f(n), \\ (8),\ (9),\ (10) \end{cases} \tag{17}$$

Moreover, the UR/DR margin of DPV at the end of $\mathcal{T}_{\text{sup}}$ should be used to mitigate SFC. In the UR scenario, there is a power decrease from $P_{e,i}(N_s)$ to $P_{m,i}(N_s)$ for each WT at the end of $\mathcal{T}_{\text{sup}}$ according to the set sequential exit strategy. Meanwhile, the DPV has an UR margin of $\left[P_{\max}^{\text{PV}} - P_e^{\text{PV}}(N_s)\right]$ according to the definition in (11) and (12). Thus, if the UR margin of DPV is larger than the total power decrease from WTs and fully released, the SFC can be basically eliminated. In the DR scenario, there is a power increase from $P_{m,i}(N_s)$ to $P_{e,i}(N_s)$ for each WT at the end of $\mathcal{T}_{\text{sup}}$ and a DPV's DR margin is $P_e^{\text{PV}}(N_s)$. Hence, the SFC mitigation conditions for UR/DR scenarios are given in (18) and (19), respectively.

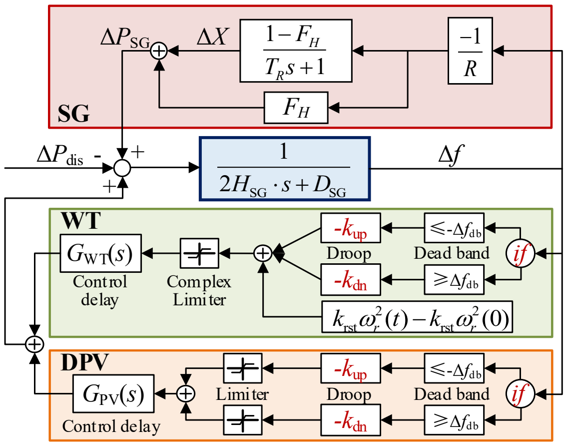

Fig. 2. SFR model with support from WT and DPV.

$$\text{UR scenario}: \begin{cases} \sum\nolimits_{i\in\mathcal{N}_{\text{WT}}}\left[P_{e,i}(N_s) - P_{m,i}(N_s)\right] \\ \leq \left[P_{\max}^{\text{PV}} - (P_{\text{base}}^{\text{PV}} - k_{\text{up}}^{\text{PV}}\Delta f(N_s))\right] \end{cases} \tag{18}$$

$$\text{DR scenario}: \begin{cases} \sum\nolimits_{i\in\mathcal{N}_{\text{WT}}}\left[P_{m,i}(N_s) - P_{e,i}(N_s)\right] \\ \leq \left[P_{\text{base}}^{\text{PV}} - k_{\text{dn}}^{\text{PV}}\Delta f(N_s)\right] \end{cases} \tag{19}$$

Finally, the WT-DPV FSC assessment model is given in (20), where the decision variables are $\{k_{\text{up},i}^{\text{WT}}, k_{\text{dn},i}^{\text{WT}}, P_{\text{base}}^{\text{PV}}, k_{\text{up}}^{\text{PV}}, k_{\text{dn}}^{\text{PV}}\}$, the intermediate variables are $\{\Delta f(n), \Delta X(n), \omega_{r,i}^2(n), P_{e,i}(n), P_{m,i}(n)\}$. Since the big-M methods are used for PWL modeling, integer variables are introduced into the model. Besides, there are Δf-related nonlinear terms such as $k_{\text{up/dn}}^{\text{WT}} \cdot \Delta f(n)$, $k_{\text{up/dn}}^{\text{PV}} \cdot \Delta f(n)$ and $(P_{\max}^{\text{PV}} - P_{\text{base}}^{\text{PV}})/|\Delta f_{\max}|$, which makes the original model almost unsolvable.

$$\begin{aligned} &\max\ k_{\text{dr}} \\ &\text{s.t.}\quad k_{\text{dr}} = k_{\text{up}}^{\text{WT}} + k_{\text{up}}^{\text{PV}} = k_{\text{dn}}^{\text{WT}} + k_{\text{dn}}^{\text{PV}}, (12)-(19) \end{aligned} \tag{20}$$

To address this solvability issue, we propose an iterative solution method based on the decoupling of SFR dynamic and WT dynamic. Specifically, we first set the WT-DPV support power to be 0 in (15) and predict the trajectories $\text{SFR}^{(0)} = \{\Delta f(n), \Delta X(n) \mid n \in \mathcal{T}_{\text{sup}}\}^{(0)}$. Then, Δf trajectory is considered to be constants in (20). After (20) is solved as a mixed integer linear programming (MILP) problem, we have $\text{FSC}^{(1)} = \{k_{\text{up},i}^{\text{WT}}, k_{\text{dn},i}^{\text{WT}}, p_{\text{base,PV}}, k_{\text{up}}^{\text{PV}}, k_{\text{dn}}^{\text{PV}}\}^{(1)}$ and related support power trajectories $\Delta P^{(1)} = \{\Delta P_{\text{WT}}(n), \Delta P_{\text{PV}}(n) \mid n \in \mathcal{T}_{\text{sup}}\}^{(1)}$. Next, $\Delta P^{(1)}$ is fed into (15) to predict $\text{SFR}^{(1)}$. Then, (20) is solved with $\text{SFR}^{(1)}$ to obtain $\text{FSC}^{(2)}$. This iteration continues until the convergence condition (21) is satisfied. From the perspective of physical principle, the power support from k_{dr} is bound to suppress frequency deviation trajectory $|\Delta f(n)|$. As the iterations progress, further minor changes in the droop gain have negligible impact on $|\Delta f(n)|$, and the aggregated FSC value stabilizes accordingly. The largest k_{dr} corresponds to the smallest $|\Delta f(n)|$.

$$\left|k_{\text{dr}}^{(k+1)} - k_{\text{dr}}^{(k)}\right| \leq 0.01 \tag{21}$$

IV. Case Study

We verify the proposed WT-DPV FSC assessment model with a modified IEEE 9-bus system with hybrid RES station in Fig.4. For each WT, the rated active power is 5 MW, R_w is 63 m, and H_{WT} is 5 s. The layout of the 20 WTs is four rows and five columns, with 6*R_w and 10*R_w spacing between the

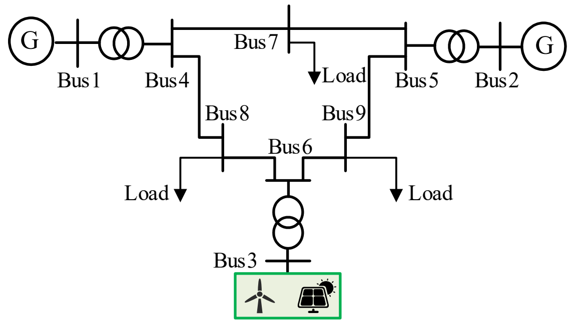

Fig. 4. Modified IEEE 9-bus system with hybrid RES station.

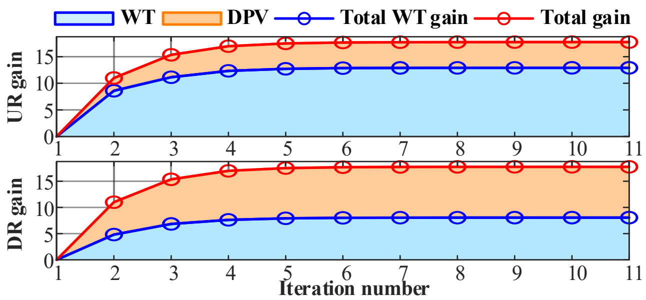

Fig. 5. Iteration process of the aggregated WT-DPV FSC.

rows and columns, respectively. Assuming total WT steady-state output power is 50MW and the ambient wind speed is 11 m/s, the reference pitch angles, rotor speeds and estimated per-WT wind speeds can be determined based on the FLORIS wake mode [12]. The maximum stable power of the aggregated DPV is 60 MW. The parameters of the aggregated SG are: H_{SG}=10, D_{SG}=0.01, F_H=0.25, T_R=8, R=0.035. Considering the worst-case disturbance size $|\Delta P_L|$=90 MW, transient simulation is performed on PSAT.

As shown in Fig.5, the iterative solution method converges after 8 times of iteration. As the frequency deviation is reduced by growing gains $\{k_{\text{up},i}^{\text{WT}}, k_{\text{dn},i}^{\text{WT}}, k_{\text{up}}^{\text{PV}}, k_{\text{dn}}^{\text{PV}}\}$, the WT-DPV k_{dr} exhibits a monotonic increase and $k_{\text{dr}}^{(8)}$=17.74. The average time taken per iteration is 3.4375 s. It can also be seen that WTs contribute the most to the UR droop gain, while DPV provides more droop gain in the DR scenario. If both WTs and DPV are required to adopt symmetric droop gains as in [2], [4], [6], the aggregated FSC k_{dr} will be 15.08% smaller, and the maximum frequency deviation will be 8.87%% larger.

Next, we examine the accuracy of the PWL WT dynamic modeling method. Fig.6 presents the simulated (red line) and model predicted (blue dotted line) extreme P_e-ω_r trajectories. Note that the simulated trajectories are obtained by setting $\{k_{\text{up},i}^{\text{WT}}, k_{\text{dn},i}^{\text{WT}}, p_{\text{base,PV}}, k_{\text{up}}^{\text{PV}}, k_{\text{dn}}^{\text{PV}}\}$ in the simulation system as the convergence results from Fig.5. It can be seen that the two kinds of trajectories are highly consistent and both reach the safety region boundary. The maximum and mean absolute ω_r prediction errors for UR and DR scenarios are (0.0026,0.0008) p.u. and (0.0022,0.0004) p.u., respectively. As for the effective safety constraints, WT-1 and WT-5 reach the upper and lower rotor speed limit for DR and UR, respectively. However, RKE potential for DR of WT-16 is not fully realized due to the lower power limit, which validates the need to fully consider WT dynamic and its safety constraints in FSC assessment. Moreover, it is observed that at the end of $\mathcal{T}_{\text{sup}}$, the relationships $P_e > P_m > P_{e,\text{rst}}$ and $P_e < P_m < P_{e,\text{rst}}$ hold for any WT in UR and DR scenarios, respectively. Therefore, when WT exits support, there must be step power decrease/increase. The negative impact under the proposed exit strategy is reduced as P_e changes to P_m rather than $P_{e,\text{rst}}$.

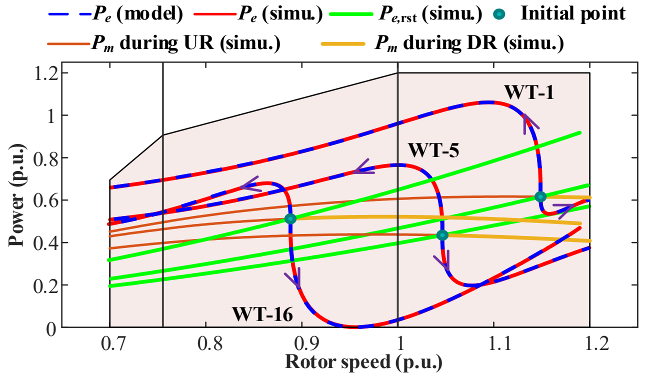

Fig. 6. Extreme P_e-ω_r trajectories of three WTs under UR and DR scenarios.

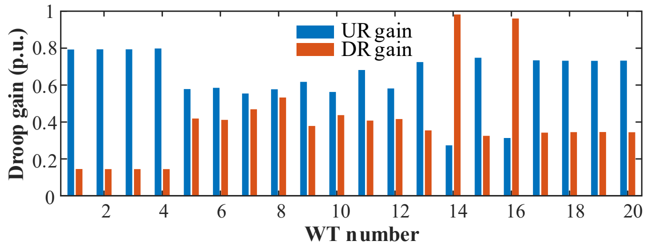

Fig. 7. Convergent UR and DR droop gains of each WT.

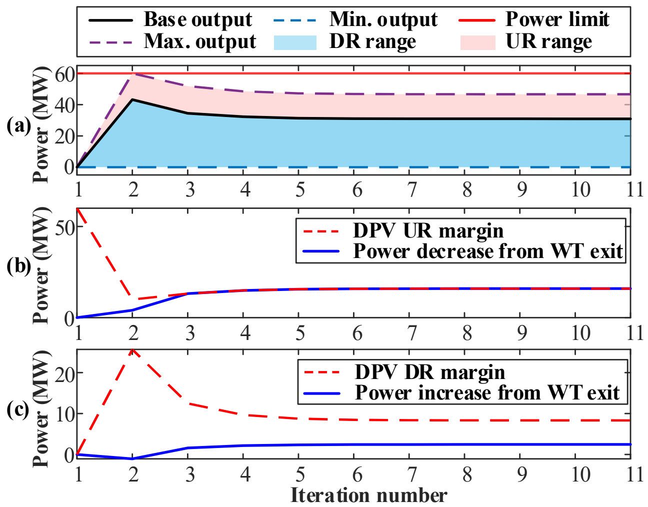

Fig. 8. Iteration process of the DPV capacity utilization.

Fig.7 shows that WTs generally have stronger UR capability than DR capability. This is mainly because the initial rotor speed is generally closer to the upper limit, which corresponds to a smaller power reduction margin. In Fig.8 (a), the width of DPV's DR range $[P_{\text{base}}^{\text{PV}} - k_{\text{dn}}^{\text{PV}}|\Delta f_{\max}|, P_{\text{base}}^{\text{PV}}]$ equals to $P_{\text{base}}^{\text{PV}}$, while the width of UR range $[P_{\text{base}}^{\text{PV}}, P_{\text{base}}^{\text{PV}} + k_{\text{up}}^{\text{PV}}|\Delta f_{\max}|]$ is smaller than $(P_{\max}^{\text{PV}} - P_{\text{base}}^{\text{PV}})$, i.e. a part of DPV curtailment is not converted into UR droop gain. The reason for this can be found in Fig.8 (b) and (c). The DPV's UR margin at the end of $\mathcal{T}_{\text{sup}}$ equals the total power decrease caused by WT exit, i.e. the constraint (18) is tight. Conversely, the DR margin at the end of $\mathcal{T}_{\text{sup}}$ is larger than the total power increase caused by WT exit, such that $k_{\text{dn}}^{\text{PV}}$ is only constrained by (12) and constraint (19) does not take effect.

With the optimal droop gains in Fig.5 and Fig.7, power system simulation is conducted to fully verify the advantages of the proposed aggregated FSC assessment model in WT FSC quantification and SFC mitigation. For comparison, two more strategies are simulated in addition to the proposed strategy (S-1). S-0: WT and DPV do not provide PFC. S-2: WT provides PFC until the end of $\mathcal{T}_{\text{sup}}$ and DPV provides

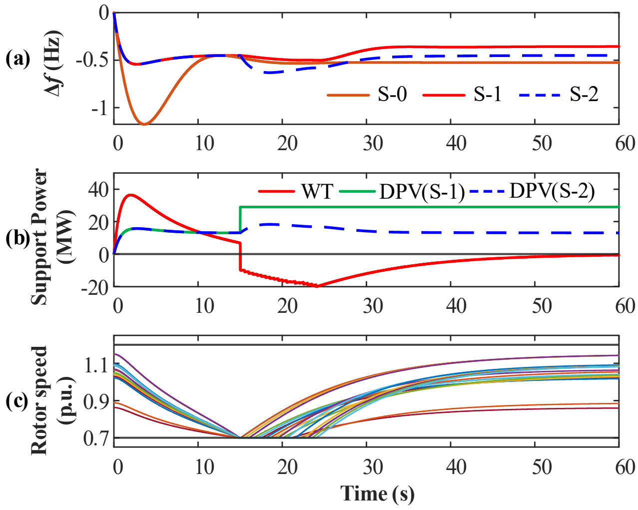

Fig. 9. Simulation results of the UR scenario.

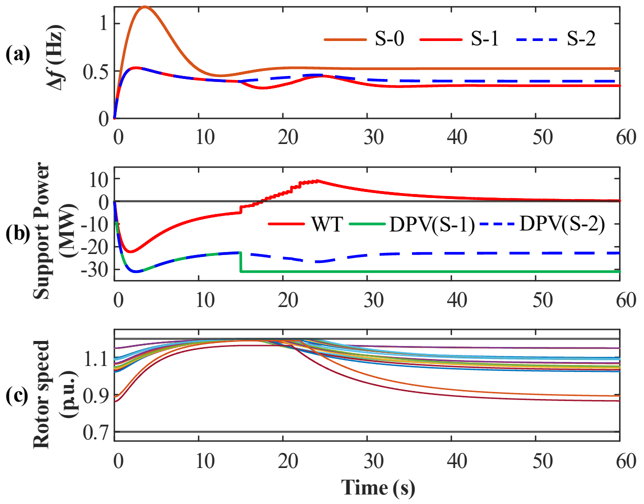

Fig. 10. Simulation results of thee DR scenario.

pure droop support without aiding WT exit. For fairness, all other settings are the same.

Fig.9 presents the simulation results of UR scenario. It can be seen that the coordinated PFC from WT-DPV significantly lifts the frequency deviation Δf. At 15 s, Δf has basically stabilized and the WTs start to disenable the PFC loop. From Fig.9 (b), the WT support power ΔP_{WT} (the same for S-1 and S-2) suddenly drops. Under S-1, the DPV fully releases the UR margin, thereby avoiding the SFC issue that occurs in the simulation under S-2. After 15 s, ΔP_{WT} continues to decrease because WTs sequentially switch their RST gains from k_{rst}' back to k_{rst}; then, $P_e = k_{\text{rst}}\omega_r^2$ makes rotor speed recover and finally ΔP_{WT} returns to 0. Fig.9 (c) shows the transition of the 20 WTs' rotor speeds (the same for S-1 and S-2). Each WT's ω_r decreases monotonically and reach the lower limit at 15 s as its RKE margin for deceleration can be exhausted according to the assessment model (20). After 15 s, each WT's ω_r remains at 0.7 p.u. until its turn to restore the RST gain.

The simulation results of DR scenario are shown in Fig.10. It can be seen that the operational logic and WT-DPV PFC performance are basically consistent with that of the UR scenario. However, according to the results in Fig.8 (c), the DR margin of DPV is greater than the total power increase caused by WT exit. Therefore, at 15 s, Δf not only does not increase but actually decreases. In addition, due to the non-negative power constraint, two WTs' RKE margin for acceleration cannot be fully utilized.

V. Conclusion

In this paper, an aggregated WT-DPV FSC assessment model is proposed to quantify the complementarity of WTs and DPVs for coordinated PFC. To accurately capture WT dynamics within the assessment framework, a PWL rotor dynamics representation and an approximation method for safety constraints are developed, enabling flexible adaptation to diverse WT operating states. The adverse impact of WTs' exit from PFC is also addressed during the assessment phase through WT-DPV coordination. Furthermore, an iterative solution approach is introduced to effectively handle the interaction between SFR dynamics and the hybrid renewable energy station. Case studies demonstrate that WT-DPV coordination can enhance the aggregated PFC provision, while the FSC assessment model ensures WT operational safety and the mitigation of SFC. Future research may explore wide-area coordinated frequency control strategies with multiple RES stations and flexible loads.

References

[1] P. Vorobev, D. M. Greenwood, J. H. Bell, J. W. Bialek, P. C. Taylor, and K. Turitsyn, "Deadbands, Droop, and Inertia Impact on Power System Frequency Distribution," *IEEE Trans. Power Syst.*, vol. 34, no. 4, pp. 3098–3108, Jul. 2019.

[2] F. Wilches-Bernal, J. H. Chow, and J. J. Sanchez-Gasca, "A Fundamental Study of Applying Wind Turbines for Power System Frequency Control," *IEEE Trans. Power Syst.*, vol. 31, no. 2, pp. 1496–1505, Mar. 2016.

[3] M. Heidari, L. Ding, M. Kheshti, X. Zhao, and V. Terzija, "Adaptive Inertial Control for Wind Turbine Generators in Fast Frequency Response Based on the Power Reduction Period Assessment," *IEEE Trans. Sustain. Energy*, vol. 16, no. 1, pp. 377–391, Jan. 2025.

[4] H. Ye, W. Pei, and Z. Qi, "Analytical Modeling of Inertial and Droop Responses From a Wind Farm for Short-Term Frequency Regulation in Power Systems," *IEEE Trans. Power Syst.*, vol. 31, no. 5, pp. 3414–3423, Sep. 2016.

[5] X. Lyu, Y. Jia, and Z. Dong, "Adaptive Frequency Responsive Control for Wind Farm Considering Wake Interaction," *J. Mod. Power Syst. Cle.*, vol. 9, no. 5, pp. 1066–1075, Sep. 2021.

[6] C. Zhao, D. Sun, X. Zhang, W. Ke, B. Hu, and H. Nian, "A Two-Stage Power Distribution Scheme of Multiple Wind Farms Participating in Primary Frequency Regulation," *IEEE Trans. Power Syst.*, vol. 38, no. 6, pp. 5009–5021, Nov. 2023.

[7] Y. Li, W. Li, D. Yang, S. Yang, G. Yan, and Z. Du, "Droop Coefficient Design of Wind Turbine Considering Rotor Speed Constraints," *IEEE Trans. Sustain. Energy*, vol. 15, no. 3, pp. 2130–2133, Jul. 2024.

[8] Z. Wang, J. Liu, L. Guo, X. Zang, X. Li, and C. Wang, "Droop-Inertia Frequency Regulation Feasible Region Assessment for Wind Farm Based on Data-Driven State Space Mapping," *IEEE Trans. Ind Appl.*, pp. 1–12, 2024.

[9] Y. Ruan *et al.*, "Online assessment of frequency support capability of the DFIG-based wind farm using a knowledge and data-driven fusion Koopman method," *Appl. Energy*, vol. 377, p. 124518, Jan. 2025.

[10] C. Wang, Y. Li, J. Liu, W. Ma, M. Yang, and T. Bi, "Chance-Constrained Primary Frequency Reserve Optimization Considering Stochastic Disturbances and Contingencies," *IEEE Trans. Power Syst.*, vol. 40, no. 4, pp. 2873–2888, Jul. 2025.

[11] S. Zhang, P. Wu, C. Lu, H. Yang, and T. Jiang, "Secondary Frequency Regulation from Aggregated Distributed Photovoltaics: A Dynamic Flexibility Aggregation Approach," *IEEE Trans. Sustain. Energy*, pp. 1–15, 2025.

[12] P. M. O. Gebraad et al., "Wind plant power optimization through yaw control using a parametric model for wake effects—a CFD simulation study," *Wind Energy*, vol. 19, no. 1, pp. 95–114, 2016.